

Performance Optimization of Gas Turbines Utilizing Four-Port Wave Rotors

E. Dempsey* and N. Müller†

Michigan State University, East Lansing, Michigan, 48824-1226, USA

P. Akbari‡ and M. R. Nalim§

Indiana University-Purdue University Indianapolis (IUPUI), Indianapolis, Indiana, 46202-5132

Many studies have demonstrated the benefits of wave rotor application in gas turbine engines. The general performance trends have been generated; however, there is a question of where the most appropriate design space is. The aim of this investigation is to answer this question by showing the generalized performance trends of several four-port wave rotor-topping configurations in a multi-dimensional space. Variables include component efficiencies, pressure ratios, and temperatures. Emphasis is on the practical application of the results in industry.

Nomenclature

Symbols and Abbreviations

<i>Gain</i>	= total wave rotor gain pressure ratio p_4/p_1
<i>OPR</i>	= overall cycle pressure ratio p_2/p_0
<i>PRW</i>	= wave rotor compression ratio p_2/p_1
<i>R</i>	= compressor pressure ratio p_1/p_0
<i>SFC</i>	= specific fuel consumption
<i>w</i>	= specific work
<i>T</i>	= temperature
η	= efficiency
<i>II</i>	= pressure ratio

Subscripts

b	= baseline (untopped) engine
comb	= combustor loss
PC	= polytropic, compressor
PT	= polytropic, turbine
th	= thermal
WE	= wave rotor expansion
WP	= wave rotor compression
1	= compressor outlet, wave rotor inlet (compression side)
2	= wave rotor outlet (compression side), combustor inlet
3	= combustor outlet, wave rotor inlet (expansion side)
4	= wave rotor outlet (expansion side), turbine inlet

* Graduate Student, Department of Mechanical Engineering, 2500 Engineering Building, Michigan State University, E. Lansing, MI, 48824-1226, AIAA Student Member.

† Assistant Professor, Department of Mechanical Engineering, 2455 Engineering Building, Michigan State University, E. Lansing, MI, 48824-1226, AIAA Member.

‡ Postdoctoral Research Associate, Department of Mechanical Engineering, Indiana University-Purdue University Indianapolis (IUPUI), Indianapolis, IN, 46202-5132, Member AIAA.

§ Associate Professor, Department of Mechanical Engineering, Indiana University-Purdue University Indianapolis (IUPUI), Indianapolis, IN, 46202-5132, Associate Fellow AIAA.

I. Introduction

There has recently been considerable interest in enhancing and even substituting conventional turbomachinery with unsteady-flow machines employing controlled compression and expansion waves.¹ This especially pertains to aerospace applications, where there have been extensive efforts in developing multi-tube or rotary pulse detonation engines (PDE)² to enhance and exceed the performance of gas turbines. As another unsteady-flow device, the wave rotor is still a favorable alternative allowing performance improvement beyond the limits set by restricted turbine inlet temperatures and other relevant design considerations. Despite considerable research yielding highly favorable results, commercialization of the wave rotor for gas turbine applications has not yet been achieved, mostly due to circumstances other than the remaining technical challenges.³

The wave rotor uses shock waves to pressurize fluids by transferring energy from a high-pressure flow to a low-pressure flow. It consists of many curved or straight channels arranged around the axis of a rotating drum or disc. Figure 1 shows⁴ a schematic of a wave rotor. LPA represents the low-pressure air received from the compressor, HPG is the high-pressure gas (exhaust) from the combustor, LPG is the low-pressure gas delivered to the turbine from the wave rotor, and HPA is the high pressure-air sent to the combustor from the wave rotor. The rotor channels are placed between two end plates with ports. The number of ports can vary, but this investigation focuses on four ports per cycle; two of them in each end plate. Each port is designed to expose the channels to the working fluids at a specific shaft angle and for a specific duration. Shock and expansion waves are initiated inside the channels by pressure differences, caused by the port opening and closing. Because the channels are exposed to both hot and cool gases, wave rotors can be naturally self-cooled. Due to the pre-expansion of the burned gases in the wave rotor besides the rotor self-cooling feature, the combustor can operate at higher temperatures without raising the turbine inlet temperature. This is especially important in gas turbine applications where the turbine inlet temperature is limited by material constraints.

The benefit of wave rotors is driven by the fact that advances in gas turbine engine technology have progressed to the point where few or little more significant increases in component efficiencies or material properties can be expected. Topping a gas turbine with a wave rotor as shown in Fig. 2 allows for significant performance enhancements and possible reduction of material costs due to changes in pressure and temperature throughout the cycle.⁵

Wave rotors have been studied since the early 1900's, and the benefits are well understood in numerous published works.^{3, 5, 6} Yet, wave rotors have not received commercialization for gas turbines. However, in the automobile industry, internal combustion engines have benefited from wave rotor addition in the form of the Comprex®.⁷ For example, 150,000 of Mazda 626 powered by a diesel engine have been supercharged with a Comprex® pressure wave supercharger. Part of the reason why there has been no commercialization of wave rotors for gas turbines may be that not much has been disseminated about the optimum design space for wave rotor application in gas turbines. Therefore, the goal of this study was to create and analyze multi-parametric performance maps for several different cases of wave rotor application to determine the optimum design space. This work is built upon a previous study⁸ where a design space was generated as a function of wave rotor compression ratio ($PRW = p_2/p_1$). In the current work, a more practical wave rotor parameter known as the gain pressure ratio ($Gain = p_4/p_1$) is used to generate the design space. This parameter represents how much the turbine inlet pressure can be increased compared to the air pressure delivered by

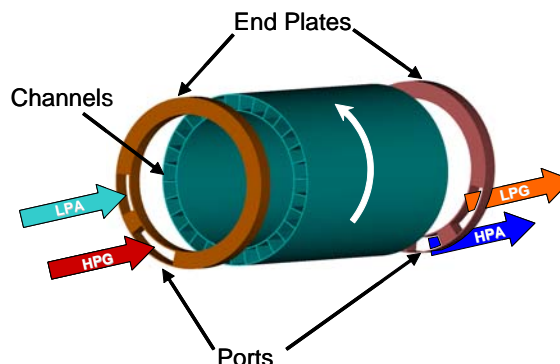


Figure 1. Schematic configuration of a wave rotor.⁴

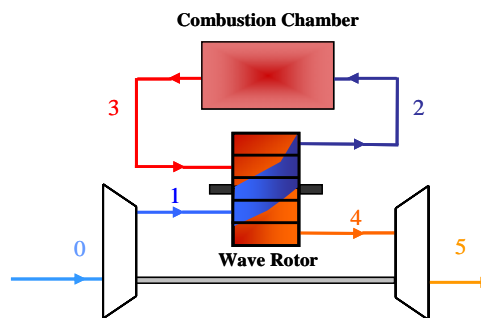


Figure 2. Wave rotor implementation in a gas turbine.

the compressor, by integrating the wave rotor into the baseline engine. Estimated values of 15-20% are theoretically possible.⁵

Similar to previous studies,⁹⁻¹² five different wave rotor-topping cases were considered in this study. The thermodynamic cycle for each case is shown in Fig. 3. Consistent with Fig. 2, the numbers represent the cycle stations, while the subscripts represent the cases. Station “0” in the cycle is the compressor inlet, “1” is the compressor outlet/wave rotor inlet (LPA), “2” is the wave rotor outlet/combustor inlet (HPA), “3” is the combustor outlet/wave rotor inlet (HPG), “4” is the wave rotor outlet/turbine inlet (LPG), and “5” is the turbine outlet.

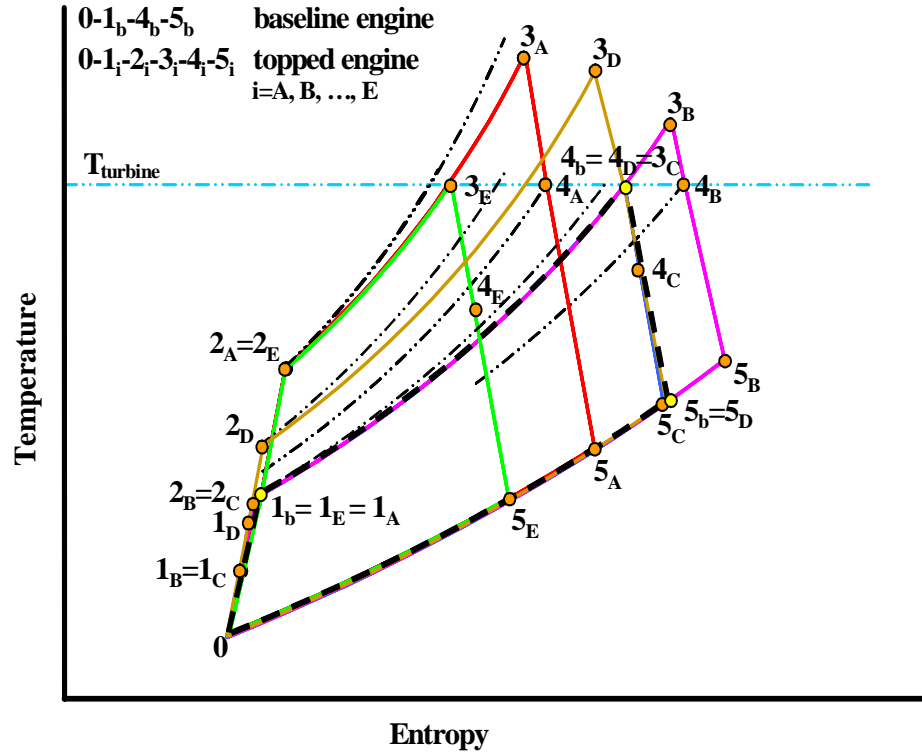


Figure 3. Schematic T-s diagrams for a baseline cycle and five different wave rotor topped cycles.

- **Case A:** Compressor is kept the same as in the baseline (untopped) engine, and turbine inlet temperature (T_{4A}) is the same as baseline turbine inlet temperature (T_{4b}). This is schematically shown in Fig. 4. The addition of a wave rotor permits combustion at higher temperature up to (T_{3A}) for the same amount of heat addition, raising the efficiency and work while reducing the fuel consumption of the cycle and the turbine exit temperature (T_{5A}).
- **Case B:** The overall pressure ratio ($OPR = p_{2B}/p_0$) and T_{4b} are kept same as in the baseline engine. More power is developed while the compressor and turbine each operate at lower pressure ratio, allowing for smaller size and less costs of the turbomachinery. With the highest turbine exit temperature (T_{5B}), this case is interesting for heat recovery. All components from the baseline engine experience modifications, as shown in Fig. 5.
- **Case C:** The combustor is unmodified (see Fig. 6) and operates with the same parameter values as in the baseline engine. Performance increases are negligible, but lower pressure ratios in the compressor and turbine exist, as well as lower turbine inlet temperature can allow for smaller size and reduced costs of the turbomachinery.
- **Case D:** The turbine operates under exact same temperatures and pressures as in the baseline engine, as shown in Fig 7. The lower pressure ratio in the compressor may allow for some size and cost savings, while some efficiency and power gains may be obtained.
- **Case E:** Compressor and cycle peak temperature at combustor exit are kept the same as in the baseline engine. While this case is similar to case A (see Fig. 4), this case reduces the thermal requirements on the turbine. Similar to cases A, B, and D, there is an increase in work and efficiency plus a decrease in fuel consumption. Further this case gives the lowest turbine exhaust temperature (T_{5E}).

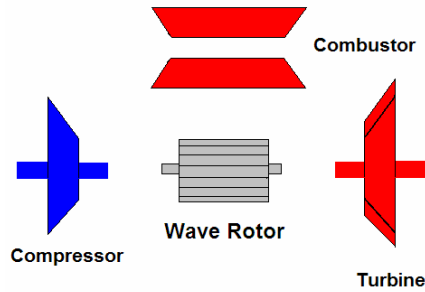


Figure 4. Cases A and E employ the same compressor as the baseline engine but larger turbine together with pressure enhanced combustor, which is also temperature enhanced for case A.

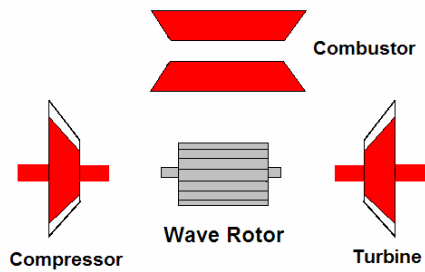


Figure 5. Case B employs a smaller compressor and turbine together with temperature enhanced combustor.

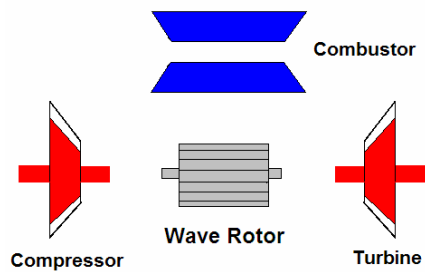


Figure 6: Case C employs the same combustor as the baseline engine but smaller compressor and turbine.

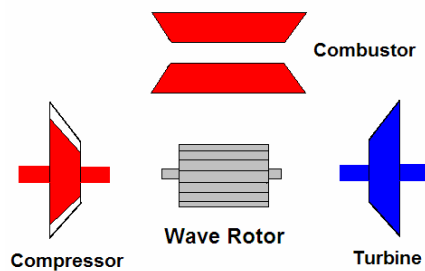


Figure 7. Case D employs the same turbine as the baseline engine but smaller compressor and pressure, besides a combustor enhanced for higher pressure and temperature.

II. Optimization Procedure

A. Theory

The thermodynamic analysis is performed by coupling the gas turbine analysis (Brayton cycle) to the wave rotor characteristic equation, introduced by Wilson and Paxson.¹³ Several steps were involved in the creation of the multi-parametric optimum performance maps. Akbari et al. have presented¹² a procedure for generating general performance maps for fixed component efficiencies and fixed turbine inlet temperature (cases A, B and D) or combustor exit temperature (cases C and E). These performance maps have shown three optimum points per wave rotor compression ratio ($PRW = p_2/p_1$). One optimum point has been for maximum thermal efficiency (η_{th}), one for maximum specific work (w), and one for minimum specific fuel consumption (SFC). In the current study, using the same thermodynamic cycle procedure, an optimization method is developed that sweeps through a wide possible design space and now per wave rotor gain pressure ratio ($Gain = p_4/p_1$), it records only these three optimum points for each turbine inlet temperature (T_4) or combustor exit temperature (T_3) and fixed component efficiencies. Hence, each of the three optimized objective parameters is a function of the component efficiencies, temperatures, and pressure ratios. In the optimization procedure for each set of these three optimum points, every independent variable except compressor pressure ratio (R) were fixed. In this respect, the major deference between the two groups of cases is that for cases A, B and D T_4 is an independent variable and T_3 is a dependent one, whereas for cases C and E T_3 is an independent variable and T_4 is a dependent one. Then through variation of R the three optimum points were found and recorded by the optimization procedure. The optimum point on the w curve is the maximum, which occurs at the R value where:

$$\delta w / \delta R = 0 \quad (1)$$

and

$$\delta^2 w / \delta R^2 < 0 \quad (2)$$

Similarly for η_{th} the optimum occurs at the R value where:

$$\delta \eta_{th} / \delta R = 0 \quad (3)$$

and

$$\delta^2 \eta_{th} / \delta R^2 < 0 \quad (4)$$

Because the optimum SFC is the minimum of the SFC values, it occurs mathematically at the R value where

$$\delta SFC / \delta R = 0 \quad (5)$$

and

$$\delta^2 SFC / \delta R^2 > 0 \quad (6)$$

With the partial derivatives in Eqs. (1-6), only one particular optimum for the independent variable R is found. The goal in the present work is to create performance maps that display only the optimum points of wave-rotor-topped gas turbines with varying combinations of component efficiencies operating under various turbine inlet and combustor outlet conditions.

While each case is different from any of the other cases, they still share some common characteristics with other cases as Fig. 4 through Fig. 7 illustrate. As observed in Ref. 12, performance data for cases A, B, and D can be displayed in one map sharing one major set of data. Similarly, performance data for cases C and E can be displayed together sharing another major set of data. The main similarity between cases A, B, and D is that they all maintain the same turbine inlet temperature T_4 as the baseline engine T_{4b} . For cases C and E, the main similarity is that the combustor end temperature T_3 is maintained the same as the baseline turbine inlet temperature T_{4b} .

The investigation applies to four-port wave rotors for both through-flow and reverse-flow configuration. In through-flow configuration, gas enters the wave rotor at one end of a channel and exits at the opposite end. In reverse-flow configuration, gas enters and exits the wave rotor at the same end of a channel.

B. Method

In order to create a performance map that displays all of the optimum points in the practical domain, layer upon layer of sets of optimum points needed to be created, each layer with a different combination of fixed engine parameters, introduced in Table 1. The most practical approach with regards to data volume and time involved was creating and running a program that steps through the various parameter values and then determining optimum

points. Only the optimum points were stored, resulting in one set for each of the two major classes of data (depending on each case) that contained all the necessary data for constructing the optimum performance maps presented in this work.

In more detail the implemented procedure follows the below steps:

1. The most inner loop of the program sweeps through the range of the compressor pressure ratio R and finds the set of the three optimum points for η_{th} , w , and SFC and stores them along with all relevant independent and dependent variables in a data matrix.
2. Then, the wave rotor compression ratio ($PRW = p_2/p_1$) is varied and the first step is repeated.
3. In an outer loop turbine inlet temperature T_4 is varied for the Cases A, B and D or combustor exit temperature T_3 for the Cases C and E and the second step containing also the first step is repeated. For each incremental temperature, the respective temperature isolines in Fig. 8 and Fig. 12 can be drawn directly as the optima values are generated.
4. To draw other isolines for other dependent values, the dependent values of the generated data matrix was searched and matching incremental values were extracted along with all the independent and dependent values of the data point and added to the plot. As the isolines are plotted in Fig. 8 and Fig. 12 the incremental search values for the wave rotor gain pressure ratio ($Gain = p_4/p_1$) were: 1, 1.2, 1.4, 1.6, 1.8 and 2.0; for the cycle peak temperature at combustor exit temperature T_3 in Fig. 8: 1400 K, 1600 K, ..., 2600 K; and for the turbine inlet temperature T_4 in Fig. 12: 1200K, 1400K, ..., 2400K.

While some results from the first two steps have been presented before,^{4, 8-12} the third and fourth step allowed the generation of maps that show only the best achievable performance (optima of three objective functions η_{th} , w , and SFC) at each compressor ratio R and the parameters in the plot at the point of consideration.

For each parameter, a realistic range of variation was investigated. For instance, the operating range for the turbine inlet temperature was set from 1000 K to 2400 K, which is the approximate limit for turbine materials and stoichiometric combustion. Table 1 also lists the range for other independent variables. Even though wave rotor compression (η_{WP}) and expansion (η_{WE}) efficiencies are in reality functions of wave rotor temperature and pressure ratios besides others as implemented by Iancu et al.,¹⁴ for simplicity, this investigation maintained $\eta_{WE} = \eta_{WP} = 0.83$, consistent with previous analytical wave rotor studies.^{13, 15}

Table 1. Independent variables and their ranges.

R	1.0-26.5
$Gain$	1.0- 2.0
T_3 (K)	1400-2600
T_4 (K)	1000-2400
Π_{comb}	0.75-0.95

III. Results and Discussion

All the data displayed in the performance maps below are optimum points. In the previous study⁸ performance optimization has been presented and discussed in respect of three possible analyses of the results: (1) the maximum “absolute performance” of the engine, (2) the maximum “absolute performance improvement” of the wave rotor-topped engine compared to the baseline engine as PRW increases, and (3) the maximum “relative performance improvement” of the topped engine compared to the baseline engine as PRW increases. This present work mainly considers the first type of analysis – the absolute performance of the engine, as it is relevant for both the design of a completely new engine and the wave rotor topping of a baseline engine. The term “optimizing” refers here to locating the maximum w and η_{th} and the minimum SFC and R . The following results are displayed and labeled as two major sets of data. The first data set is obtained from the optimization for a fixed (constraint) turbine inlet temperature T_4 (Figs. 8-11). This is a one typical constraint for the design of a new engine and for the wave-rotor-topping of a baseline engine in cases A, B, and D. The second data set is obtained for a fixed (constraint) temperature at combustor outlet T_3 (Figs. 12-15) that may be understood as maximum allowable cycle peak

temperature. This can be another possible constraint for the development of a new engine and is relevant for the wave-rotor-topping of a baseline engine in cases C and E.

A. Optimum Performance Maps

Figures 8 and 12 show the performance maps that only contain performance optimized points obtained through the here described optimizing procedure. Figure 8 is relevant if the turbine inlet temperature is fixed (cases A, B and D) and Fig. 12 is valid when the cycle peak temperature (assumed at combustor outlet) fixed, which includes cases C and E. The values of the constant parameters are shown in the upper left corner. For the presented plots they are $\eta_{PC} = \eta_{PT} = 0.9$ and $\Pi_{comb} = 0.95$. In both performance maps, optimum thermal efficiency lines for constant T_4 are shown as bold light green lines, and thermal efficiency lines of constant T_3 are shown as thin dark green lines. Specific work lines of constant T_4 are shown as bold blue lines, and specific work lines of constant T_3 are shown as thin dark blue lines. Similarly, specific fuel consumption lines of constant T_4 are shown as bold red lines, and specific fuel consumption lines of constant T_3 are shown as thin brown lines. In the bottom part of both Fig. 8 and Fig. 12 and enlargement of map for specific fuel consumption is shown for clarity of it. All lines of constant *Gain* are shown as thin broken pink lines. For the case of no combustor pressure losses, lines of constant T_4 and constant T_3 would intersect at *Gain* = 1. However, this investigation deals with non-ideal components, and there are losses from many factors including boundary layer diffusion, leakage, and secondary flows.

While the detailed data are not the same in Figs. 8 and 12 the general trends are similar. For all topping cases, as T_4 increases for constant *Gain*, also η_{th} , w , *OPR*, and *R* increases, while *SFC* decreases. The same is true for increasing T_3 . However, following a line with constant T_3 in direction of increasing *Gain* shows a decrease in η_{th} and w , and an increase in *SFC*. The opposite is true following a line of constant T_4 in direction of increasing *Gain*. Along both lines always *R* decreases with increasing *Gain*. In other words, in all cases (Figs. 8 and 12) it can be observed that adding a wave rotor with increasing *Gain* results for the same turbine inlet temperature always in reduced *R* and increased T_3 while all performance parameters (η_{th} , w , *SFC*) improve. Further comparing inclination of the lines of constant *Gain* it can be seen that with a high wave rotor gain, the same increase in *R* results in much more improvement of η_{th} , w , and *SFC*. At high temperatures of T_4 or T_3 the same wave rotor gain yields much more reduction of *R*, that means probably much more size reduction of the compressor.

B. Changes of Optimum Performance Maps

The general optimum performance maps in Figs. 8 and 12 still have three main parameters kept constant as they are listed in the upper left corner ($\eta_{PC} = \eta_{PT} = 0.9$ and $\Pi_{comb} = 0.95$). Now in Fig. 9 through Fig. 11 for optimization with fixed T_4 and in Fig. 13 through Fig. 15 for optimization with fixed T_3 , the effect is shown how the performance maps in Figs. 9 and 12, respectively, would distort when these parameters change too. For better readability lines of constant T_3 are omitted. Only a simplified quadrilateral base region is shown by bold solid lines that indicate the upper and lower limits of $T_4 = 1600\text{K}$, $T_4 = 1200\text{K}$, *Gain*=2, and *Gain*=1. In reality, the sides of the quadrilateral are not straight but slightly curved as it can be seen in Fig. 8 and Fig. 12. The fixed values of the base region are now all lowered by 0.05 resulting in $\eta_{PC} = \eta_{PT} = 0.85$ and $\Pi_{comb} = 0.85$ as shown in the upper right corner of Fig. 9 through Fig. 11 and Fig. 13 through Fig. 15. This is to obtain a realistic range of display for these parameters (η_{PT} , η_{PC} , and Π_{comb}), which are now all varied by +/- 0.1 in value, indicating how the limits move and skew. This adds another three dimensions creating seven dimensional performance maps (Figs. 9-11 and 13-15).

The effect of the polytropic compressor efficiency η_{PC} is shown by dashed lines, of the polytropic turbine efficiency η_{PT} by solid thin lines, and of the combustor pressure loss Π_{comb} by dotted lines. The plots Figs. 9-11 and 13-15 were generated by using the same procedure as for generating those in Figs. 8 and 12. Only after creation of the base plot this complete procedure was repeated six times each with a new set of fixed parameters (η_{PT} , η_{PC} , and Π_{comb}) in which always only one of the three parameters η_{PT} , η_{PC} , and Π_{comb} was changed by a difference of 0.1 in value. From each such generated performance map the quadrilateral with the same boundaries ($T_4 = 1600\text{K}$, $T_4 = 1200\text{K}$, *Gain*=2, and *Gain*=1) was selected and all seven were superimposed. Arrows were added that indicate the direction of the distortion of the four corners of the base quadrilateral with the change of the parameters η_{PT} , η_{PC} , and Π_{comb} . The new regions are still quadrilateral.

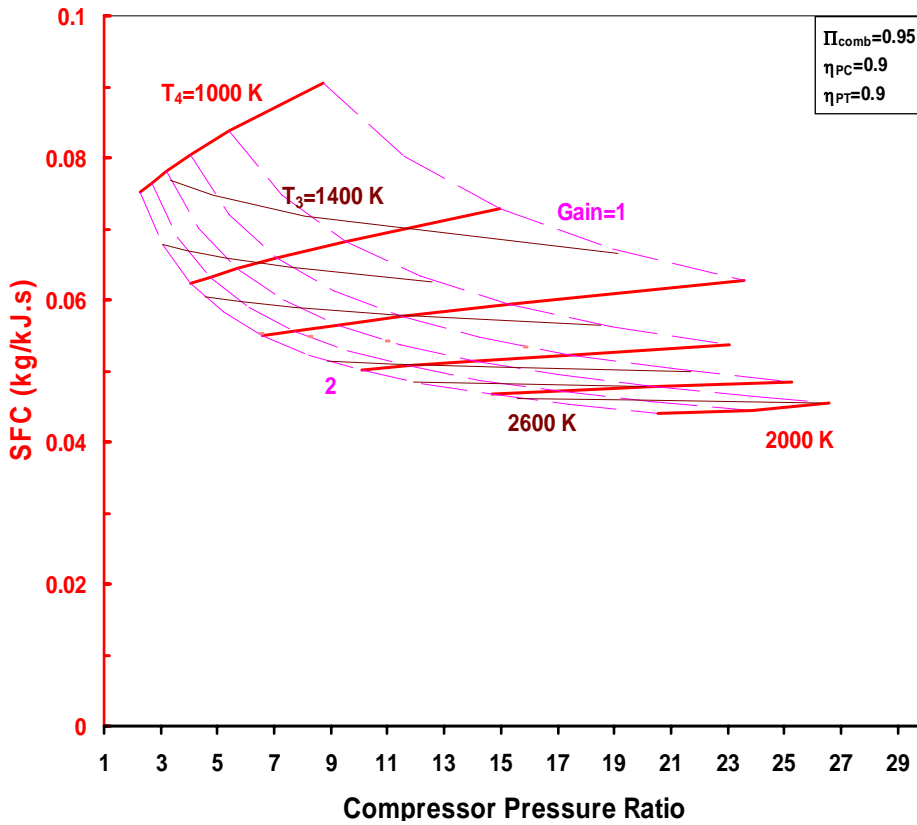
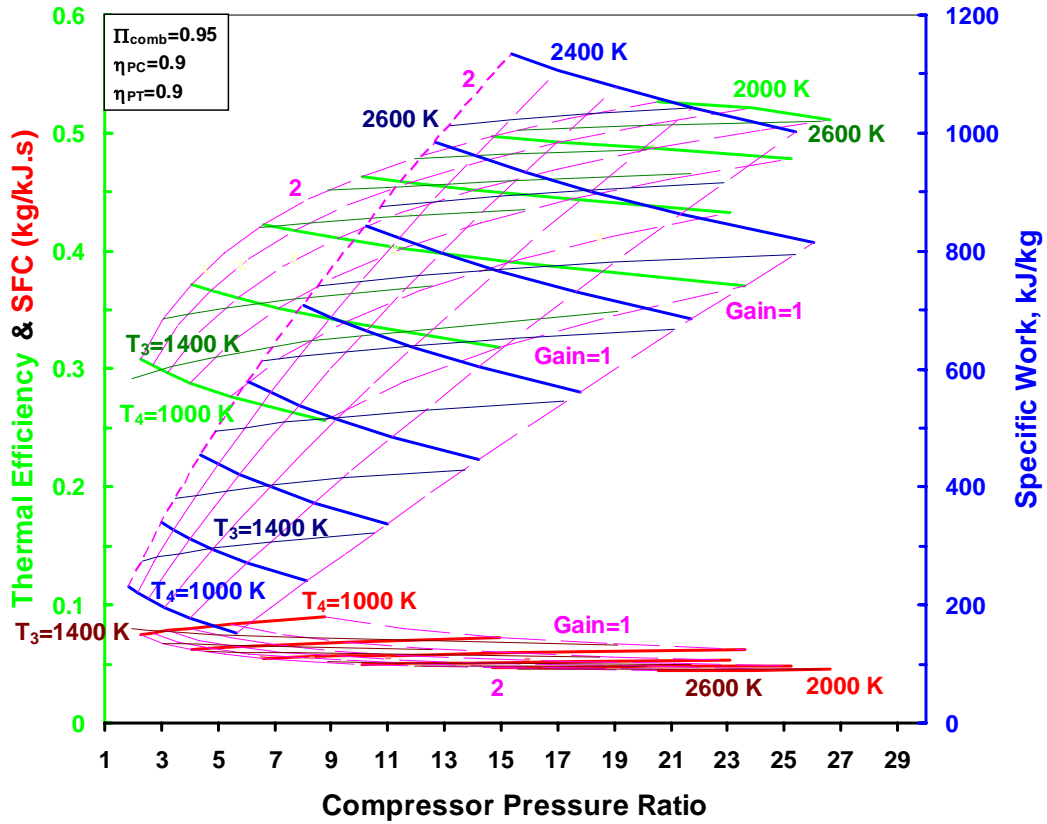


Figure 8. Optimized points for various constraint turbine inlet temperatures T_4 (cases A, B, and D).

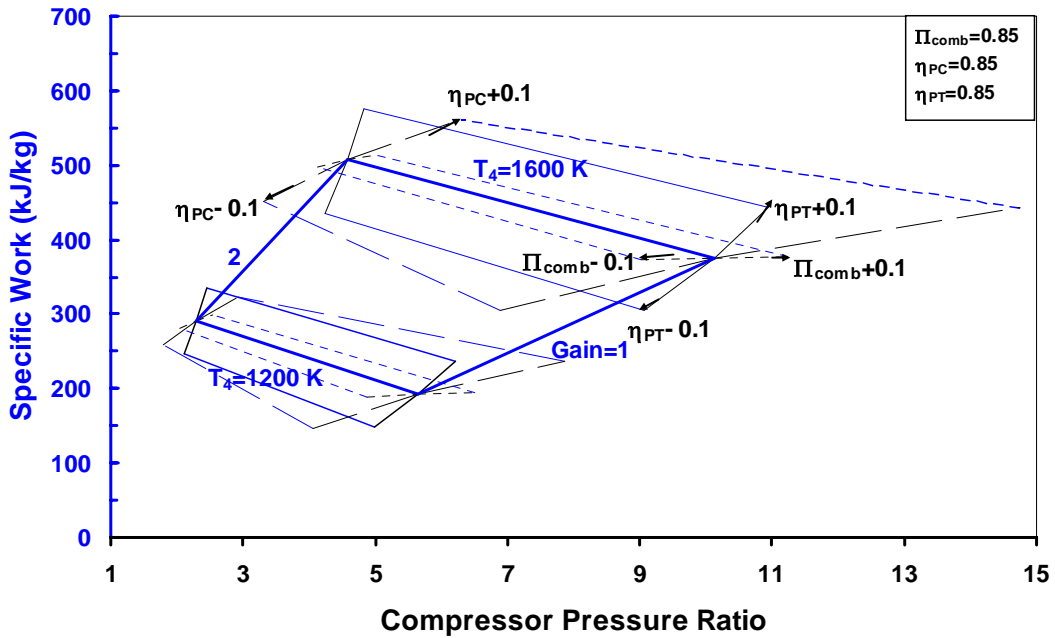


Figure 9. Optimum specific work for variation of polytropic compressor efficiency, polytropic turbine efficiency, and combustor loss for cases A, B, and D.

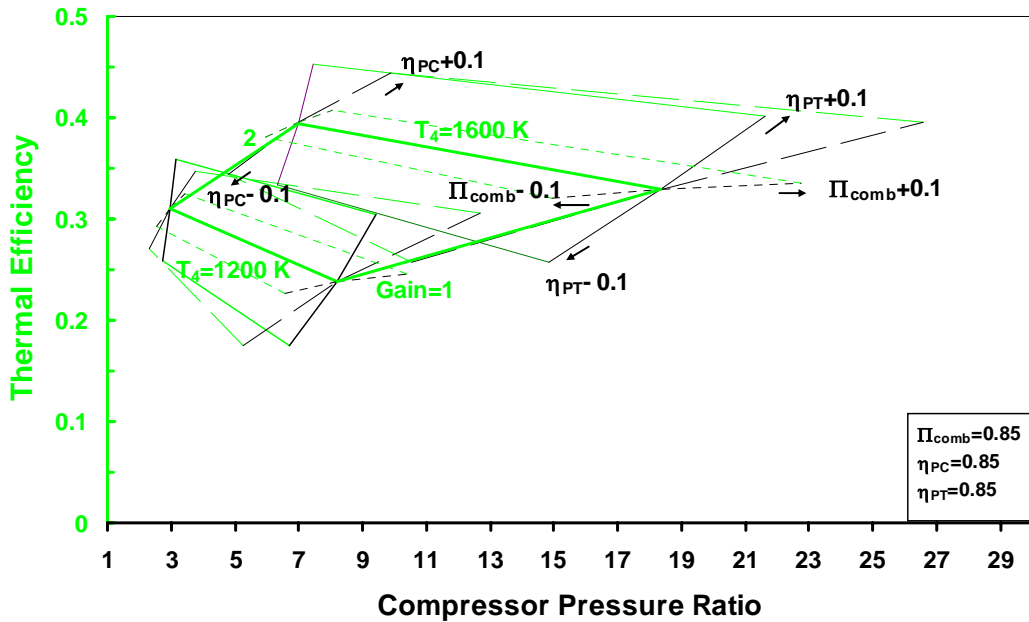


Figure 10. Optimum thermal efficiency for variation of polytropic compressor efficiency, polytropic turbine efficiency, and combustor loss for cases A, B, and D.

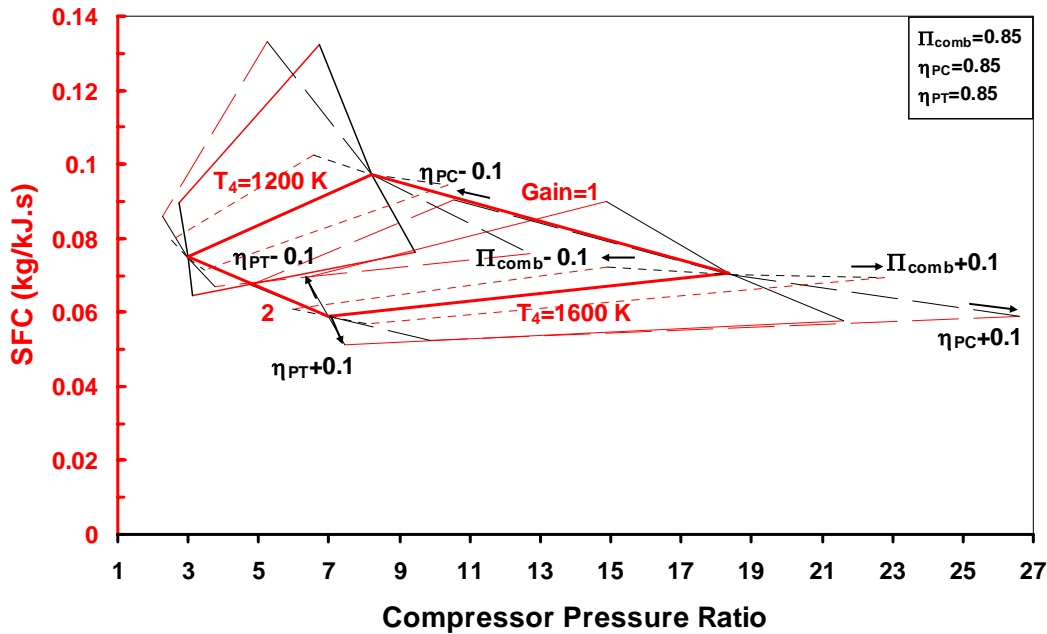


Figure 11. Optimum specific fuel consumption for variation of polytropic compressor efficiency, polytropic turbine efficiency, and combustor loss for cases A, B, and D.

Also when the fixed parameters η_{PT} , η_{PC} , and Π_{comb} are changed, still the same general trends are true as they were described above for Figs. 8 and 12. However the changes of the parameters η_{PT} , η_{PC} , and Π_{comb} all show a different effect.

Overall the greatest distortion is generated by changes in the polytropic compressor efficiency η_{PC} . Changes of η_{PC} impact heavily the optimum Compressor ratio R . An increase of η_{PC} always results in improved performance (η_{th} , w , SFC) and increased optimum compressor ratio R . This effect is the strongest at high temperatures and there at low gain. This also indicates that with a high wave rotor *Gain* the increase of optimum compressor ratio is much less than with low *Gain* or no wave rotor when the compressor polytropic efficiency can be increased, meaning the the compressor does not need to increase in size so much for reaching optimum. Further, this proves that operating at a lower compressor efficiency will not change the optimum performance as much at low T_4 and high *Gain* than it would at high T_4 and low *Gain*.

Much alike the scenario for η_{PC} , an increase in polytropic turbine efficiency η_{PT} also always results in improved performance (η_{th} , w , SFC) and increased optimum compressor ratio R , with the difference that the ratio of both is much more to the benefit of improved performance with less increase in R . Especially with high wave rotor *Gain* the effect on optimum R with changing η_{PT} is almost negligible, suggesting improved robustness of operation.

By comparison, the effect of changing Π_{comb} on optimum performance is much less than the effect of changing either η_{PC} or η_{PT} . Though small, the greatest effect on performance can be seen at low T_4 and high *Gain*.

Changes in Π_{comb} mainly affect directly the optimum compressor pressure ratio R . The effect on R is similar to the effect of varying η_{PC} or η_{PT} , and the largest effect is likewise found at high T_4 and low *Gain*. Although it is almost insignificant and accompanied with significant increase of optimum R , in most cases reducing the combustor losses improves performance as expected. The only exception is the effect on specific work w , where less combustor loss (greater Π_{comb}) often reduces the specific work here shown for high temperatures and low *Gain*. Only for low temperatures and high *Gain*, this is reversed to some improved specific work when combustor losses are reduced. This is typically connected with small optimum R , showing an advantage of wave rotor application for typically small gas turbines with low T_4 and small R .

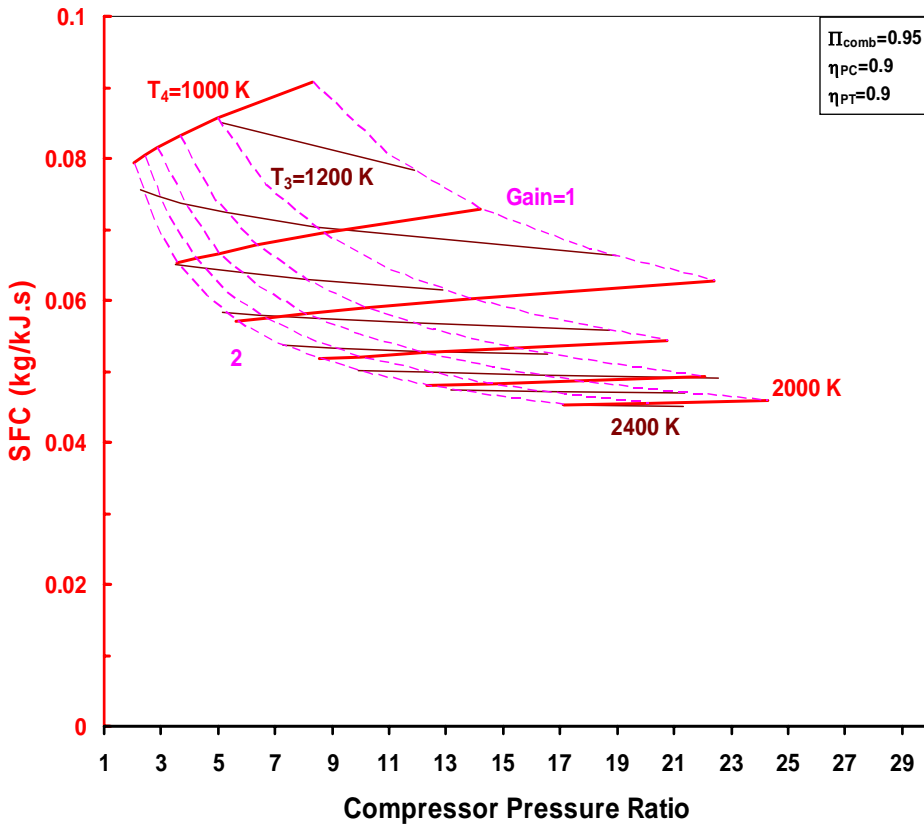
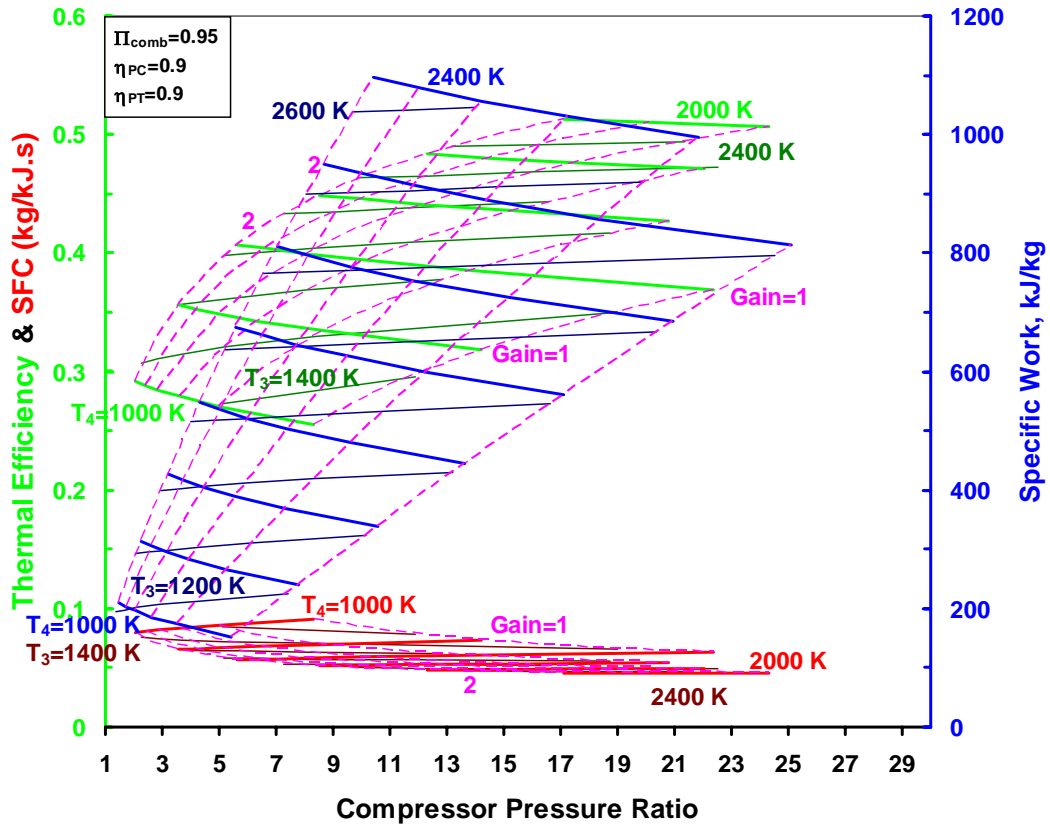


Figure 12. Optimized points for various constraint combustor outlet temperatures T_3 (cases C and E).

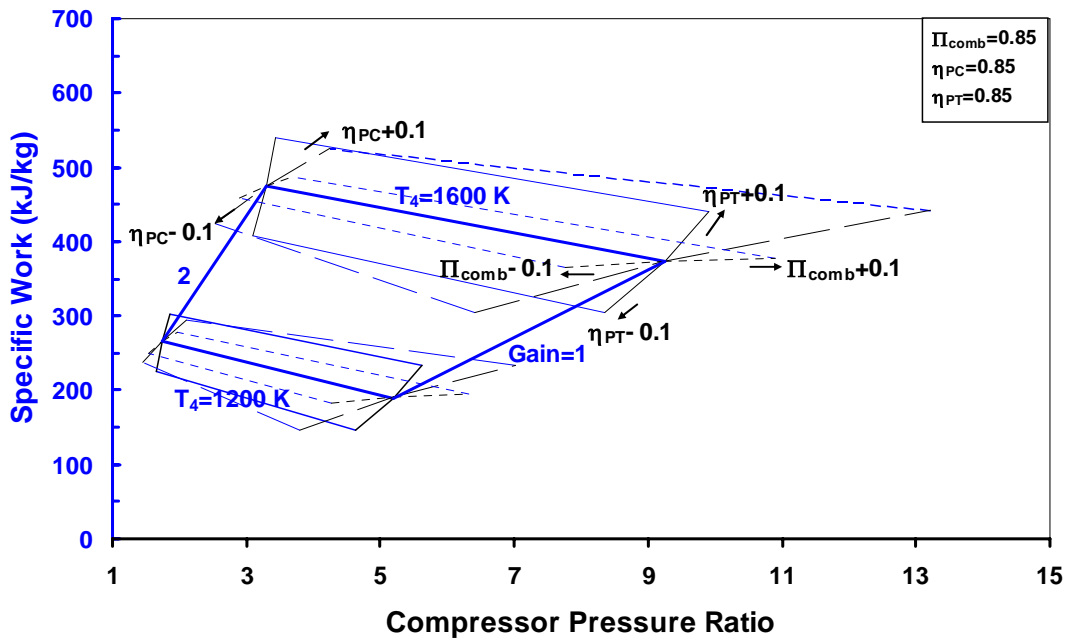


Figure 13. Optimum specific work for variation of polytropic compressor efficiency, polytropic turbine efficiency, and combustor loss for cases C and E.

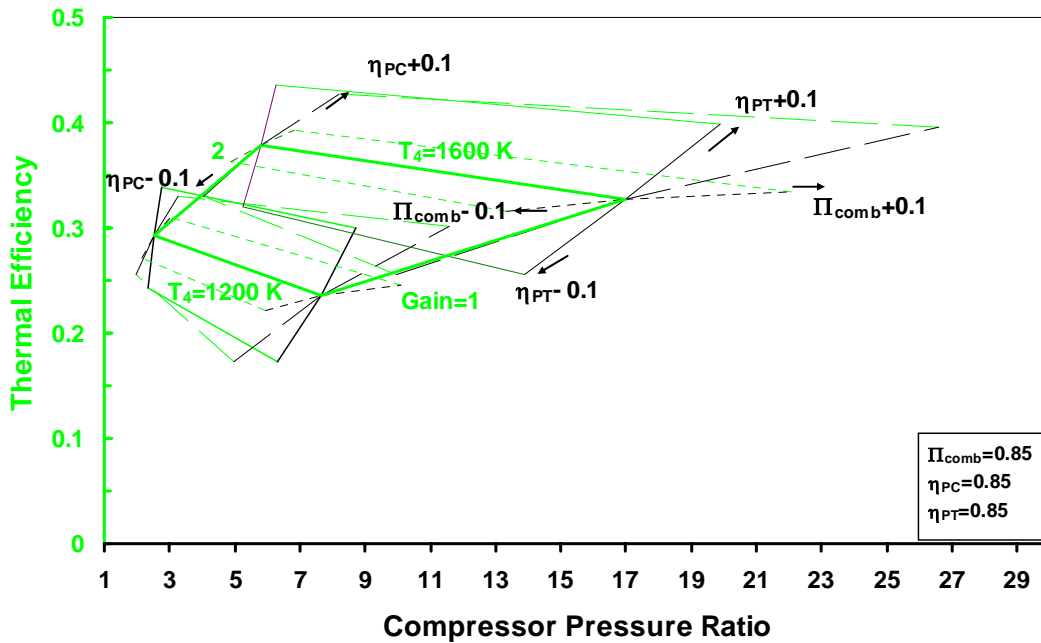


Figure 14 . Optimum thermal efficiency for variation of polytropic compressor efficiency, polytropic turbine efficiency, and combustor loss for cases C and E.

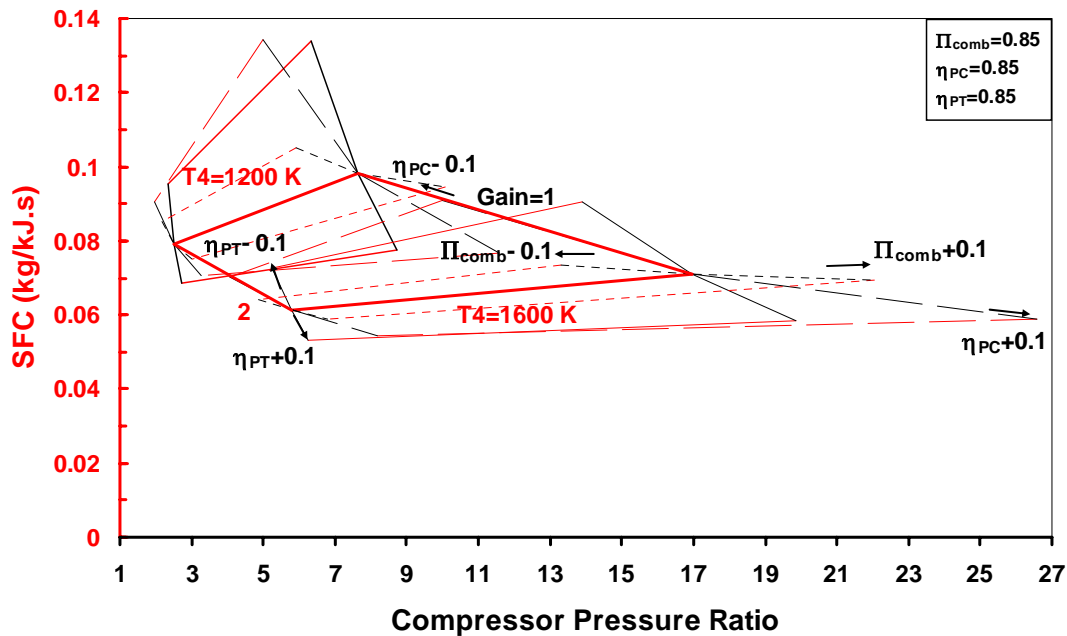


Figure 15. Optimum specific fuel consumption for variation of polytropic compressor efficiency, polytropic turbine efficiency, and combustor loss for cases C and E.

IV. Conclusions

A series of optimum points was obtained for three objective functions of wave rotor-topped gas turbine performance: thermal efficiency, specific work, and specific fuel consumption that were expressed as functions of the independent variables T_3 , T_4 , $Gain$, η_{PC} , η_{PT} , and Π_{comb} . A total of five cases were investigated; three which maintain the same turbine inlet temperature as the baseline engine (cases A, B and D) and two which maintain the same combustor outlet temperature as the baseline engine (cases C and E). The conclusions are:

1. There are two main sets of optimum points: one for cases A, B, and D, and one for cases C and E.
2. The optimum trends for specific work, thermal efficiency, and specific fuel consumption are the same for all cases.
3. High values of T_4 , η_{PC} , η_{PT} , and Π_{comb} result in high gains for the objective functions, while low values of those parameters result in small optimum compressor pressure ratios.
4. Among η_{PC} , η_{PT} , and Π_{comb} , η_{PT} has the greatest effect on the objective functions and the least on the compressor pressure ratio R , whereas Π_{comb} has the least effect on the objective functions and almost only affects R .
5. The most positive effect of increased Π_{comb} (less combustor pressure loss) on the objective functions is seen at high $Gain$ and low T_4 , whereas otherwise it is almost negligible.
6. At high $Gain$ (with wave rotor topping) the absolute performance gain per improved component parameter η_{PC} , η_{PT} , and Π_{comb} is considerable greater for much less required increase of compressor pressure ratio R .
7. At low T_4 and high $Gain$, reduction of engine component efficiencies is possible without sacrificing optimum performance as much.

Wave rotor topping of gas turbine engines is beneficial throughout a wide range of gas turbine sizes, efficiencies, and operating conditions. Because the focus of the investigation is on wave rotor enhancement of gas turbine engines, the most significant conclusions can be drawn from the performance improvement of objective functions. Similar to the results from a previous investigation, small gas turbines with low component efficiencies, low temperatures may benefit most from wave rotor-topping.

References

- ¹Azoury P. H., *Engineering Applications of Unsteady Fluid Flow*, John Wiley and Sons, New York, 1992.
- ²Roy, G. D., Frolov, S. M., Borisov, A. A., and Netzar, D. W., "Pulse Detonation Propulsion: Challenges, Current Status, and Future Perspective," *Progress in Energy and Combustion Science*, Vol. 30, No. 6, 2004, pp. 545-672.
- ³Akbari, P., Nalim, M. R., and Müller, N., "A Review of Wave Rotor Technology and Recent Developments," ASME Paper IMECE2004-60082, 2004. Also in print *ASME Journal of Engineering for Gas Turbines and Power*, 2006.
- ⁴Iancu, F., "Integration of a Wave Rotor to an Ultra-Micro Gas Turbine," Ph.D. Thesis, Michigan State University, MI, 2005.
- ⁵Welch, G. E., "Overview of Wave-Rotor Technology for Gas Turbine Engine Topping Cycles," *Novel Aero Propulsion Systems International Symposium*, The Institution of Mechanical Engineers, 2000, pp. 2-17.
- ⁶Shreeve, R. P., and Mathur, A., *Proceeding ONR/NAVAIR Wave Rotor Research and Technology Workshop*, Report NPS-67-85-008, Naval Postgraduate School, Monterey, CA, 1985.
- ⁷Berchtold, M., "The Comprex®," *Proceeding ONR/NAVAIR Wave Rotor Research and Technology Workshop*, Report NPS-67-85-008, Naval Postgraduate School, Monterey, CA, 1985, pp. 50-74.
- ⁸Dempsey, E., Akbari, P., Müller, N., and Nalim, M. R., "Optimum Applications of Four-Port Wave Rotors for Gas Turbines Enhancement" *17th International Symposium on Air Breathing Engines*, ISABE Paper 2005-1214, 2005.
- ⁹Akbari, P., and Müller, N., "Performance Improvement of Small Gas Turbines Through Use of Wave Rotor Topping Cycles," ASME Paper GT2003-38772, 2003.
- ¹⁰Akbari, P., "Performance Prediction and Preliminary Design of Wave Rotors Enhancing Gas Turbine Cycles," Ph.D. Thesis, Michigan State University, MI, 2004.
- ¹¹Akbari, P., Müller, N., and Nalim, M. R., "Performance Improvement of Recuperated and Unrecuperated Microturbines Using Wave Rotor Machines," 2004 ASME-ICED Spring Technical Conference, Japan, 2004.
- ¹²Akbari, P., Müller, N., and Nalim, M. R., "Performance Enhancement of Microturbine Engines Topped with Wave Rotors," *ASME Journal of Engineering for Gas Turbines and Power*, Vol. 128, No. 1, 2006, pp. 190-202.
- ¹³Wilson, J., and Paxson, D. E., "Jet Engine Performance Enhancement Through Use of a Wave-Rotor Topping Cycle," NASA TM-4486, 1993.
- ¹⁴Iancu, F., Piechna, J., Dempsey, E., and Müller, "Ultra-Micro Wave Rotor Investigations," *Proceeding 5th International Workshop on Micro and Nanotechnology for Power Generation and Energy Conversion Applications (PowerMEMS)*, Tokyo, 2005, pp 93-96.
- ¹⁵Fatsis, A., and Ribaud, Y., "Thermodynamic Analysis of Gas Turbines Topped with Wave Rotors," *Aerospace Science and Technology*, Vol. 3, No. 5, 1999, pp. 293-299.